agriculture

MDPI

Article

Simulation Research on Cotton Stalk Cutting and Crushing Based on ANSYS/LS-DYNA and Field Experiments

Peng Wang [1,2], Xuegeng Chen [1,3,*] and Haojun Wen [1,3]

[1] College of Mechanical and Electrical Engineering, Shihezi University, Shihezi 832000, China; wangp@stu.shzu.edu.cn (P.W.); mj2859903@shzu.edu.cn (H.W.)
[2] Xinjiang Uygur Autonomous Region Research Institute of Measurement & Testing, Urumqi 830011, China
[3] Key Laboratory of Northwest Agricultural Equipment, Ministry of Agriculture and Rural Affairs, Shihezi 832000, China
* Correspondence: chenxg130@shzu.edu.cn

Abstract: In order to solve the problem of high straw content in recovered residual film and the low rate of qualified straw crushing in combination with a front-mounted cotton-straw-crushing device, the cutting and crushing mechanisms of cotton stalks were studied based on ANSYS/LS-DYNA. The height h and dip angle α of the fixed blade were determined to be 30 mm and 75° through a finite element analysis. On the basis of the device design, explicit dynamic models of the cutting and crushing of a single cotton stalk were established based on ANSYS/LS-DYNA. The results of the dynamic analysis revealed the cutting mechanism of the cotton stalk, and the influences of the cutting edge angle γ and front baffle height h_1 on cotton stalk cutting were studied by using single-factor simulation tests. An edge angle of $\gamma = 45°$ and a height of $h_1 = 265$ mm were determined. Meanwhile, the mechanism of cotton straw crushing was revealed, and the motion states of the straw were studied at different times. The results of the simulation experiments on the influence of the cutter shaft's rotational speed showed that with an increase in the cutter shaft's speed, the rate of qualified crushing and the removal rate were both increased. At the design speed of $n = 1800$ RPM, the rate of qualified crushing was 84.6%, and the removal rate was 95.1%. Then, field experiments were carried out. The test results were as follows: the stubble height was 8.0 cm, the rate of qualified straw crushing was 91.8%, the clearance rate of film-surface impurities was 92.3%, and the film content was 3.6%, which met the working quality requirements (not less than 85%) of NYT 500-2015: "Operating quality for straw-smashing machines".

Keywords: front-mounted cotton-straw-crushing device; simulation research; ANSYS/LS-DYNA; cutting mechanism; crushing mechanism; field experiment

Citation: Wang, P.; Chen, X.; Wen, H. Simulation Research on Cotton Stalk Cutting and Crushing Based on ANSYS/LS-DYNA and Field Experiments. *Agriculture* **2023**, *13*, 1268. https://doi.org/10.3390/agriculture13061268

Academic Editor: Galibjon M. Sharipov

Received: 27 May 2023
Revised: 15 June 2023
Accepted: 16 June 2023
Published: 19 June 2023

1. Introduction

Plastic-film-mulching technology can significantly increase crop yield and water use efficiency, especially in dryland agriculture [1]. As an important cash crop in Xinjiang, cotton has a long history of the application of mulch-planting technology. However, the use of a vast amount of plastic film in agriculture has resulted in serious plastic-residue pollution [2]. In recent years, China has attached great importance to plastic-residue pollution; as such, residual-film-recycling machines have continued to develop and mature. The problem of residual-film recovery has gradually evolved into the problem of the secondary utilization of recovered residual film [3]. It is not conducive to the reuse of residual film if its impurity rate is too high. So, impurity removal is the key issue that must be solved in the mechanized recovery of residual film. In this study, impurities mainly refer to cotton straw, cotton leaves, cotton (scattered), and so on.

In order to address the problem of the high impurity content in residual film, many scholars have performed exploratory research. Xie et al. researched a screen-hole-blockage-clearing device for a residual-film–impurity wind separator, and the main structure and

working parameters affecting the screen-hole-clogging situation were determined through a theoretical analysis and computational fluid-dynamics simulations [4]. Peng et al. designed a stripping and impurity-removal device that was mainly composed of film-stripping tooth plates, two wind-collecting hoods, and two centrifugal fans [5]. Cao et al. designed a device for picking up residual film with a hook-and-tooth chain rail to solve the current problems of high impurity content and the poor reliability of chain-harrow-type residual-film-recovery machines when picking up residual film [6]. Shi et al. realized residual-film–impurity separation by utilizing the difference in the suspending velocities and settlement laws of different materials in an air medium, and a drum-sieve-type air-separation device was designed [7]. Li et al. proposed a washing, separation, and cleaning method based on an impeller drive and jet impact, and they designed and developed a washing and separation device [8]. To sum up, the removal of impurities has usually been studied in experiments. Cotton straw is an important part of the impurities in film residue, but few studies have focused on the mechanism of removing cotton straw. Our team proposed a front-mounted cotton-straw-crushing device, and residual-film–impurity separation was realized before the recovery of the residual film. The mechanism of removing light impurities on a film's surface was analyzed [3]. As a composite material with a complex structure, cotton stalks have a large deformation and material fracture in the process of cutting and crushing, so it was necessary to use simulation software to conduct visualization research. The ANSYS/LS-DYNA solution software can be used to study high-speed collisions, impact loads, and nonlinear material problems in nonlinear structures, and it has been widely used in agricultural mechanization engineering. For example, it was used to solve the problems of low net harvesting rates, high loss rates, and uneven stubble heights during the harvest of laver. A rigid–flexible coupling model related to the interaction between the cutting mechanism and the laver was constructed based on ANSYS/LS-DYNA [9]. By using ANSYS/LS-DYNA to simulate the rock-breaking process, Duan et al. analyzed the influence of the geometric configuration, including the blade width and blade fillet, on rock-breaking behavior [10]. The process of picking safflower was simulated with the ANSYS/LS-DYNA software, and the structure and motion parameters of the picking device were continuously adjusted until the safflower ball and branch reached the ideal picking position [11]. Taking the branch of the "shixia" variety of longan as the test object, ANSYS/LS-DYNA was used to perform a finite element simulation of the branch-cutting process [12]. In order to analyze the influence of changes in the working parameters of a serrated rotary cutter on the cutting resistance of soybean and to optimize the combinations of parameters of the cutter, the soybean-cutting process of the serrated rotary cutter was simulated with ANSYS/LS-DYNA, and the changes in the cutting resistance throughout the whole cutting process were analyzed [13]. A rigid–flexible coupling model related to the interaction between the cutting mechanism and the laver was constructed based on ANSYS/LS-DYNA in order to solve the problems of low net harvesting rates, high loss rates, and uneven stubble heights during the harvest of laver [9]. Therefore, it is feasible to simulate the cutting and crushing process for cotton stalks based on finite element simulations with ANSYS/LS-DYNA.

In this study, the cutting and crushing mechanisms of cotton stalks are analyzed based on ANSYS/LS-DYNA, which is conducive to understanding the process of removing cotton straw. Finally, field experiments were carried out to verify the effects of straw removal under different working conditions.

2. Materials and Methods

2.1. Structure of the Front-Mounted Cotton-Straw-Crushing Device

As an important part of the "4JMLE-210 agricultural residual film recycling machine" [3], the front-mounted cotton-straw-crushing device was mainly composed of a drive shaft, belt transmission system, tensioning mechanism, straight pipe section, cutter blade, fixed blade, crushing chamber, etc., as shown in Figure 1. Before the recovery of

residual film, the cotton straw should be crushed and thrown out to create good conditions for the subsequent recovery of residual film.

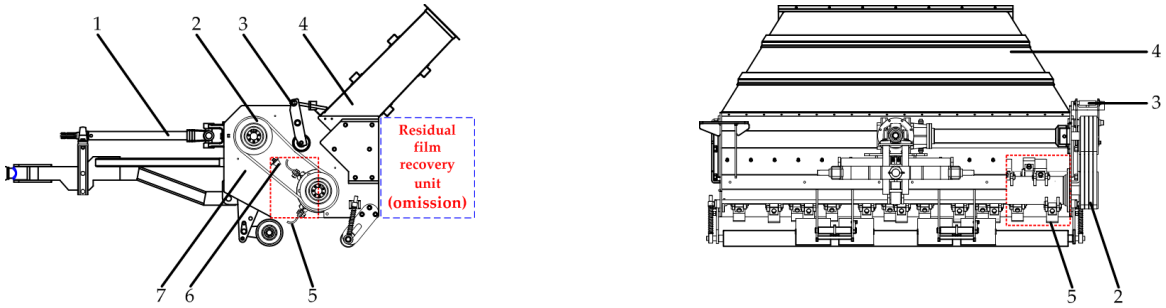

(**a**) Side view (**b**) Front view

Figure 1. Diagram of the structure of the front-mounted cotton-straw-crushing device: 1. Drive shaft; 2. Belt transmission system; 3. Tensioning mechanism; 4. Straight pipe section; 5. Cutter blade; 6. Fixed blade; 7. Crushing chamber.

2.2. Working Principle

Because of the high stiffness of cotton straw, the rotary cutting method without support was selected in this study. There were two options for this rotary cutting method: first, the rotation direction of the cutter shaft could be the same as that of the tractor's driving wheel (positive rotation); and second, the rotation direction of the cutter shaft could be opposite to the direction of the tractor's driving wheel (reverse rotation) [14]. If positive rotation was selected, the crushed straw would be directly scattered on the surface of the residual film, which would not be conducive to the removal of cotton straw. Therefore, the reverse-rotation cutting method was selected.

When working, the tractor would output power through the drive shaft, gearbox transmission system, and belt drive system to drive the cutter shaft. With the advance of the machine, cotton stalks would be instantly cut off at the bottom, and the broken straw would enter into the crushing chamber under the action of the cutter blade, where it would be crushed into small segments or fibers under the comprehensive action of cutting, tearing, and rubbing with the combination of the cutter blade and fixed blade. Finally, the crushed straw would be evenly spread at the rear of the machine under the joint action of airflow and centrifugal force.

3. Design of the Key Components and Parameter Determination

3.1. Cutter Blade

A tool apron was welded to the cutter shaft. The cutter blade was connected to the connector with a bolt and nut, and the connector was linked to the tool apron with a pin shaft, as shown in Figure 2a. The type of cutter blade directly affected the reliability and operation of the whole machine [15]. In addition, it was necessary for the high-speed rotating cutter blade to crush and pick up the cotton stalks.

As shown in Figure 2b, if the cutter blade's height was too great, the structure would be expanded, and the stability of the device would deteriorate. If it was too small, it would be necessary to increase the rotational speed of the cutter shaft to crush the cotton straw, which would increase power consumption. The height of the cutter blade L_0 was designed to be 120 mm in this study. Under the condition that the strength was guaranteed, it was necessary for the thickness of the cutter blade d_0 to be between 5 mm and 10 mm [16]. In order to increase the moment of inertia of the blade, prevent the blade from deformation, and ensure a high safety factor, d_0 was designed to be 8 mm [17]. If the cutter blade's width D_0 was too large, this would result in the overlapping of adjacent blades, increased wind resistance, and increased power consumption. However, if the width of the cutter blade D_0 was too small, this would result in a gap between adjacent blades during operation,

and the air speed on the film surface would not be able to reach the purpose of removing light impurities. Because the axial distance of the adjacent tool apron was 70 mm, D_0 was designed to be 70 mm. The blade was bent with a bending radius of 40 mm. So, the length of the cutter blade b_0 was 40 mm. γ was the cutting edge angle of the cutter blade, which had a significant influence on the contact force when cutting cotton stalks in the following simulation study.

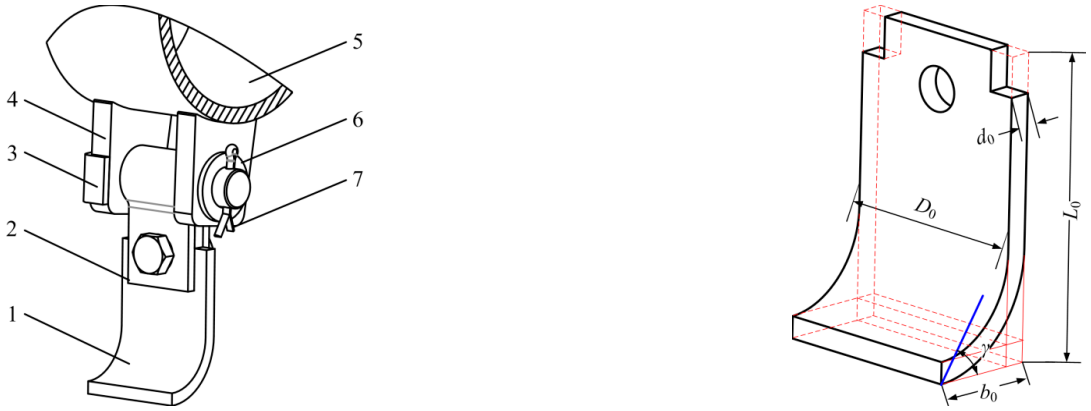

(**a**) Assembly (**b**) Cutter blade

Figure 2. Structural design of the cutter blade: 1. Cutter blade; 2. Connector; 3. Pin shaft; 4. Tool apron; 5. Cutter shaft; 6. Round washer; 7. Cotter pin. D_0, b_0, d_0, and L_0 are the width, length, thickness, and height of the blade, respectively, and γ is the edge angle of the blade.

The cutter blades and the cutter shaft formed a multi-rigidity rotor. Theoretically, its moment of inertia was not a constant, but the cutter shaft quickly returned to the equilibrium position when rotating at a high speed due to its reasonable arrangement [18]. According to experience [19], 28 groups of cutter blades were arranged, the axial distance between each two adjacent groups was equal, and the radial angle was 90°, as shown in Figure 3. This arrangement had 7 blades working at the same time, which could reduce the vibration and force on both ends of the cutter shaft and improve the service life of the machine.

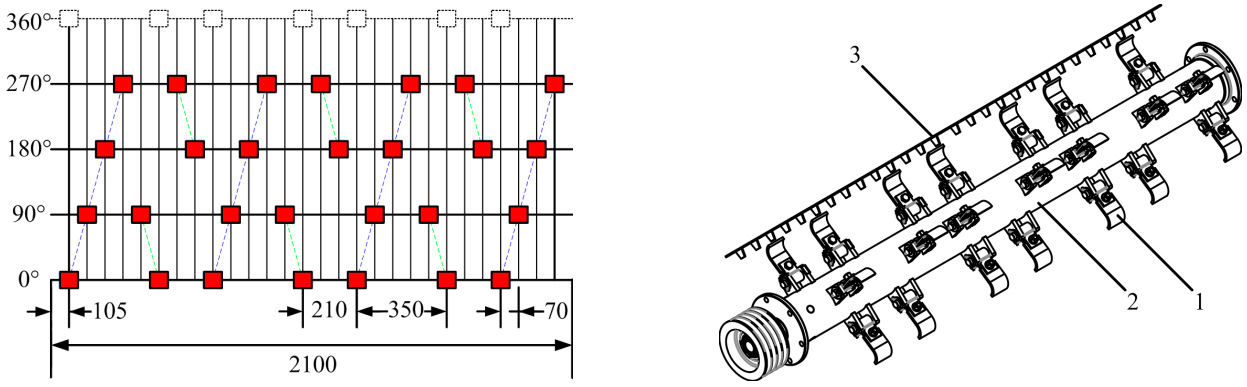

Figure 3. Schematic diagram of the array of cutter blades: 1. Cutter blade; 2. Cutter shaft; 3. Fixed blade.

3.2. Fixed Blades

A row of fixed blades was installed in the crushing chamber to assist in straw crushing, as shown in Figure 4a. The fixed blades were welded to the steel plate, which was fixed to the upper inner wall of the crushing chamber with bolts. In order to prevent excessive deformation of the fixed blade during the working process and interference with the high-

speed cutter blade, the thickness of the fixed blade t was determined to be 4 mm, the length of the two adjacent fixed blades d was determined to be 70 mm, and the width of the steel plate b was determined to be 40 mm. The fixed blades were quenched to ensure that they had enough wear resistance and stiffness. In addition, the dip angle α and height h of the fixed blade were determined by using finite element analysis.

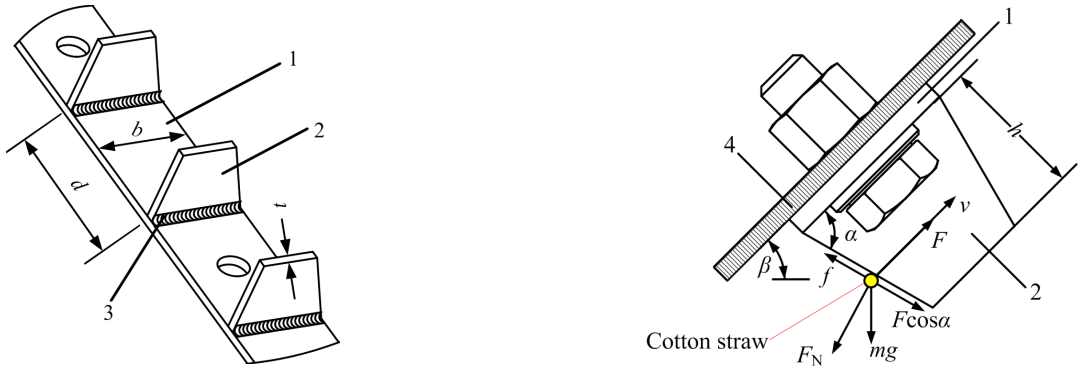

(**a**) Steel plate and fixed blade (**b**) Mechanical analysis of cotton straw

Figure 4. Design of the fixed blade for crushing: 1. Steel plate; 2. Fixed blade; 3. Positive fillet weld; 4. Upper inner wall of the crushing chamber. b is the width of the steel plate, d represents the two adjacent fixed blades, t represents the fixed blade, α is the dip angle, h is the height of the fixed blade, F is the inertial force, F_N is the normal cutting force of the cotton straw, f is the friction force, v is the velocity of the cotton straw before the collision, β is the throwing angle of the crushing chamber, and m is the mass of the cotton straw.

The cotton straw collided with the fixed blade at a high speed, and a force analysis is shown in Figure 4b. At the moment of contact between the straw and the fixed blade, the inertial force F was generated, the collision time was Δt, the change in the velocity of the cotton straw before and after the collision was Δv, and the cotton straw was subjected to the normal cutting force F_N of the fixed blade. According to the conservation of momentum, the following relationship existed:

$$\begin{cases} F \approx \frac{m \cdot \Delta v}{\Delta t} \\ F_N = F \sin \alpha \end{cases} \quad (1)$$

The normal force F_N was the main force involved in straw crushing; then, the dip angle α was as large as possible (not more than 90°). When the high-speed collision time Δt approached 0, the inertial force F approached infinity; it was considered that F was much larger than mg, and the gravitational effect could be ignored at this time. There was a critical state:

$$\begin{cases} f = F \cos \alpha \Rightarrow \\ \mu \cdot F_N = F \cos \alpha \Rightarrow \\ \tan \alpha = \frac{1}{\mu} \end{cases} \quad (2)$$

where μ was the static friction factor between the cotton straw and fixed blade, and μ = 0.64 (experimentally measured). By using Formula (2), α = 57.3° could be calculated. This is because a larger value of α was more conducive to cutting, so the value of α was selected within the range of 57.3° to 90° for the finite element simulation.

Then, 65Mn was selected as the fixed blade's material; according to GB/T 699-1999 on "high-quality carbon structural steel", the following mechanical properties of 65Mn were used: the tensile strength [σ_b] was 735 MPa, the yield strength [σ_s] was 430 MPa, the density ρ was 7.9 × 10^3 kg/m^3, Poisson's ratio v was 0.3, the elastic modulus E was 206 GPa, and the shear modulus G was 79.38 GPa. The failure load at the bottom of the cotton stalk was 3.35 kN [20], and the same force value was applied to the contact surface of the

fixed blade. The maximum stress and maximum deformation were used as experimental response indexes to reflect the strength of the fixed blade; thus, they were used as the target parameters [21]. Because the thickness of the fixed blade t was determined to be 4 mm, the other structural parameters were the key factors that affected its strength. So, according to the actual situation, the strength of the fixed blade and practical premises were ensured, and the height h between 0.5b and 1.5b and a dip angle α between 60° and 90° were used as independent variables for the finite element analysis, as shown in Figure 5.

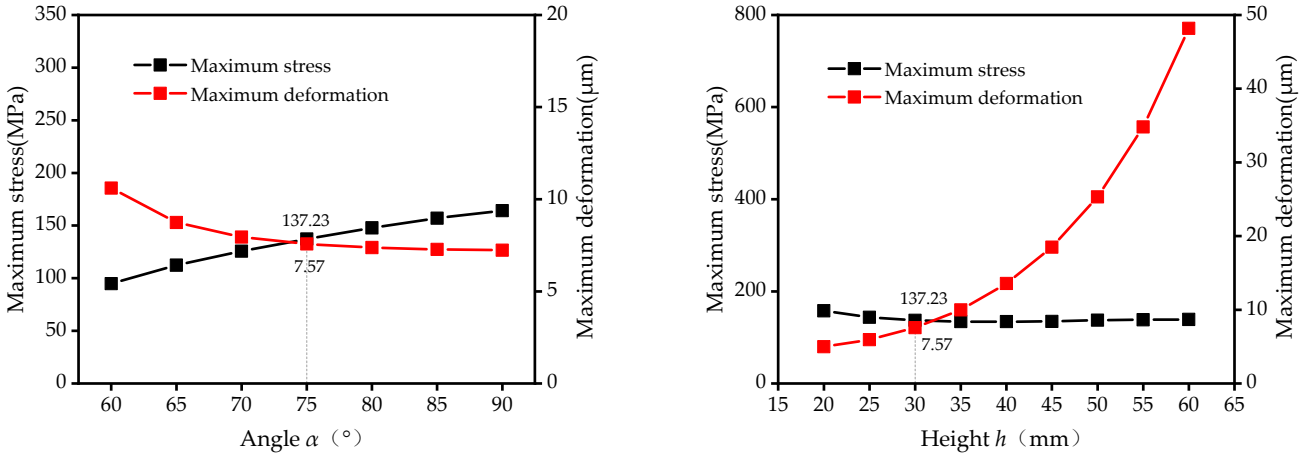

Figure 5. Single-factor finite element analysis of the fixed blade.

When the height h was greater than 30 mm, the maximum stress tended to be stable, and the maximum deformation obviously increased with the gradual increase in the height. Meanwhile, when the angle α was greater than 75°, the maximum deformation tended to be stable, and the maximum stress slowly increased with the gradual increase in the angle. The finite element analysis results for the fixed blade when h = 30 mm and α = 75° are shown in Figure 6. The stress concentration and maximum deformation of the blade were mainly distributed in the root and top of the blade. The maximum stress was 137.23 MPa, and the maximum deformation was 0.008 mm. Compared with the tensile strength of the selected material ($[\sigma_b] \geq 735$ MPa) and the minimum tensile strength of the weld metal ($[\sigma_B] \geq 43$ kgf/mm^2 = 420 MPa [22]), it could be seen that the fixed blade that was designed was safe.

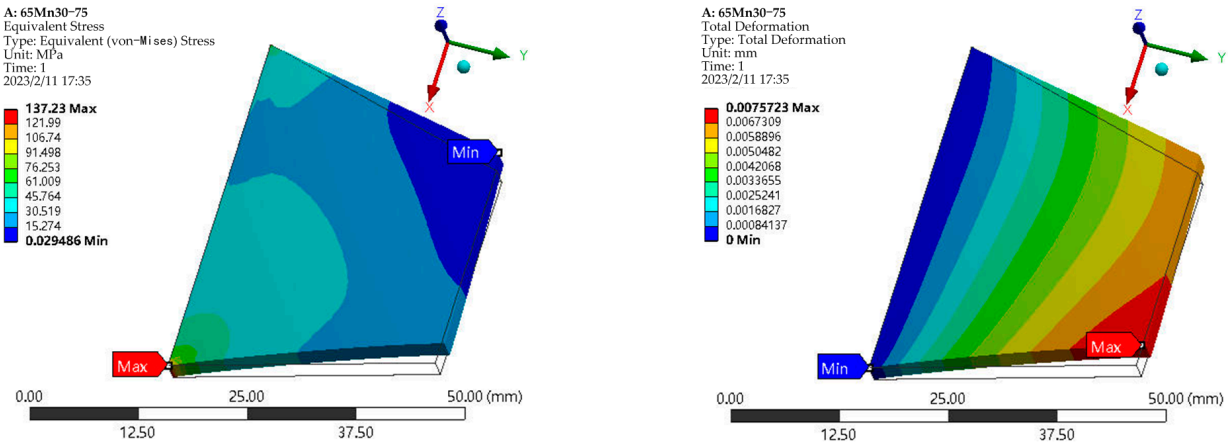

(**a**) Equivalent stress (**b**) Total deformation

Figure 6. Results of finite element analysis of the fixed blade.

In addition, processing technology could also be used to improve the mechanical properties of the parts [23]. In fact, the fixed blade that we designed was also heat-treated before assembly.

3.3. Crushing Chamber

The main design parameters of the crushing chamber included h_1 (or h_2), which was the height of the front (or rear) baffles from the ground, as well as L_1 (or L_2), which was the clearance between the front baffles (or rear baffles) and the edge of the cutter blade, as shown in Figure 7. If L_1 was too large, the straw-crushing effect was not good; otherwise, if L_1 was too small, this would easily result in blockage. The clearance between the upper wall of the crushing chamber and the edge of the cutter blade was designed to be equal to L_1. So, we calculated L_1 according to Formula (3).

$$L_1 = h + t + D \tag{3}$$

where h is the height of the fixed blade, and h = 30 mm; t is the thickness of the steel plate, and t = 4 mm; and D is the safety gap, the purpose of which is to avoid collisions between the moving cutter blade and the fixed blade (the diameter of a cotton stalk was taken as the safety gap).

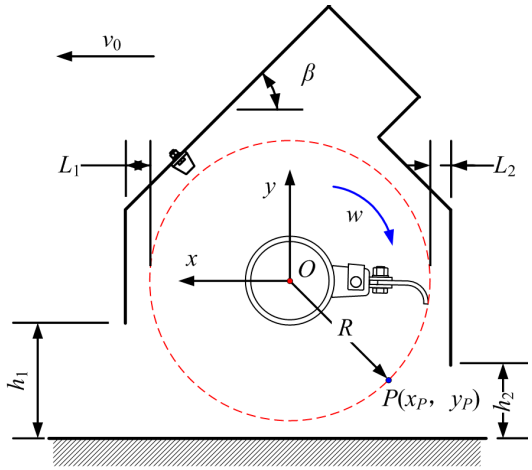

Figure 7. Structural design of the crushing chamber: h_1 (or $h_{2)}$ is height of the front (or rear) baffles from the ground, and L_1 (and L_2) is the clearance between the front baffles (or rear baffles) and the edge of the cutter blade. β is the throwing angle of the crushing chamber, v_0 is the forward speed of the device, w is the angular speed of the cutter shaft, R is the radius of the motion of the cutter blade's edge, xOy is a rectangular coordinate system with the center of the cutter shaft as the origin, and $P(x_P, y_P)$ is a point on the motion path of the cutter blade's edge.

According to the literature [20], the bottom diameter of a cotton stalk ranges from 9.25 mm to 13.58 mm, and the average diameter is 11.54 mm. So, L_1 = 30 mm + 4 mm + 11.54 mm = 45.54 mm, and this calculation was integrated into the design as L_1 = 45 mm. In addition, if L_2 was too large, a broken cotton stalk would be brought back to the film's surface, which was not conducive to residual-film recovery. In the preliminary design of this device, L_2 was slightly less than L_1, so L_2 = 40 mm was used.

When a cotton stalk was effectively cut with the cutter blade at point A, the cut stalk obtained an instantaneous velocity V_A at point A, and its direction was inclined upwards along the direction of the stalk and perpendicular to l_{OA}. The partial velocities of V_A along the x and y axes were V_{Ax} and V_{Ay}, as shown in Figure 8. The conditions for the stalk to enter the crushing chamber smoothly were

$$V_{Ay} \geq V_{Ax} \tag{4}$$

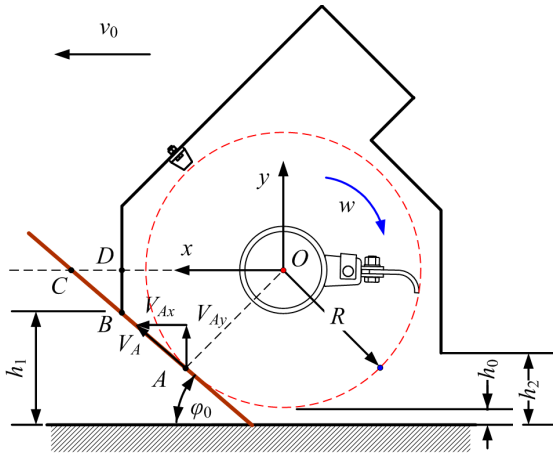

Figure 8. Instantaneous velocity analysis: h_1 (or h_2) is the height of the front (or rear) baffles from the ground, and L_1 (or L_2) is the clearance between the front baffles (or rear baffles) and the edge of the cutter blade. h_0 is the height of the edge of the cutter blade from the ground, v_0 is the forward speed of the device, w is the angular speed of the cutter shaft, R is the radius of the motion of the cutter blade's edge, xOy is a rectangular coordinate system with the center of the cutter shaft as the origin, V_A is the velocity of the cut stalk, V_{Ax} and V_{Ay} are the partial velocities of V_A along the x and y axes, and φ_0 is the angle between the cotton stalk and the ground.

At the critical state when $V_{Ax} = V_{Ay}$, $\varphi_0 = 45°$; then, the following existed:

$$\begin{cases} l_{BD} = l_{CD} \\ l_{OC} = l_{CD} + l_{DO} = \sqrt{2} l_{OA} = \sqrt{2} R \\ l_{DO} = L_1 + R \\ l_{BD} + L_1 = \left(\sqrt{2} - 1\right) R \end{cases} \tag{5}$$

Because the minimum speed was $v_{\min}$ = 48 m/s for the unsupported cutting of cotton stalks [24], the rotary radius of the cutter blade was determined to be R = 265 mm. Substituting L_1 = 45 mm and R = 265 mm into Formula (5), l_{BD} = 65 mm was obtained. h_0 was the distance between the cutter blade's edge and the ground, as shown in Figure 8. The height h_0 could be changed with a depth-limiting adjustment mechanism (60 mm $\leq h_0 \leq$ 100 mm), and h_0 = 80 mm was used in the preliminary design. Then, the height of h_1 = 280 mm was also determined for the preliminary design in a subsequent explicit dynamic simulation. Specific requirements for the height of h_2 are rarely reported. Here, h_2 = 180 mm, so both side plates would be the same distance from the ground.

4. Analysis and Establishment of an Explicit Dynamic Model

4.1. Geometric Model of a Cotton Stalk

The structural characteristics of cotton stalks were abstracted into a mechanical model that could be studied and analyzed. Then, relevant assumptions were made about cotton stalks—they have a straight, cylindrical, linear elastic structure with transverse anisotropy, and microscopic discontinuities and microscopic defects were ignored [25]. According to the literature [20], the average height of cotton is 634.16 mm, and the average diameter is 11.54 mm, as mentioned above. In this section, the cotton stalk model is considered a cylinder with a length of 650 mm and a diameter of 12 mm, as shown in Figure 9.

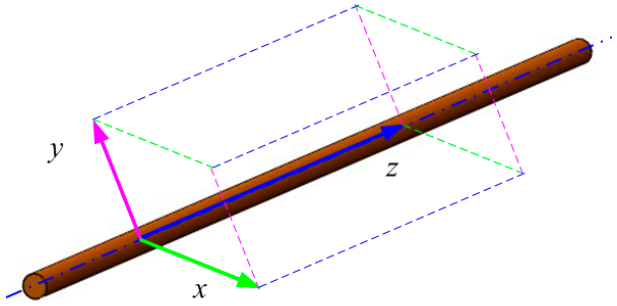

Figure 9. Geometric model of a cotton stalk: z is the axial direction of the cotton stalk model, and x and y represent the two directions of the cross-section of the cotton stalk model, respectively.

4.2. Cutting Model and Meshing Grid

Only one cutter blade was selected for the simulation analysis, and the front baffle was simplified to the form of a rigid beam body. The cutter blade and the connector formed a new assembly, and the tool apron was merged with the cutter shaft. A corresponding constraint was applied between the connector and the tool apron to replace the pin shaft, while the chamfer and filleted corner were ignored. It was assumed that the cutter shaft was always at the same height during the cutting process, as shown in Figure 10.

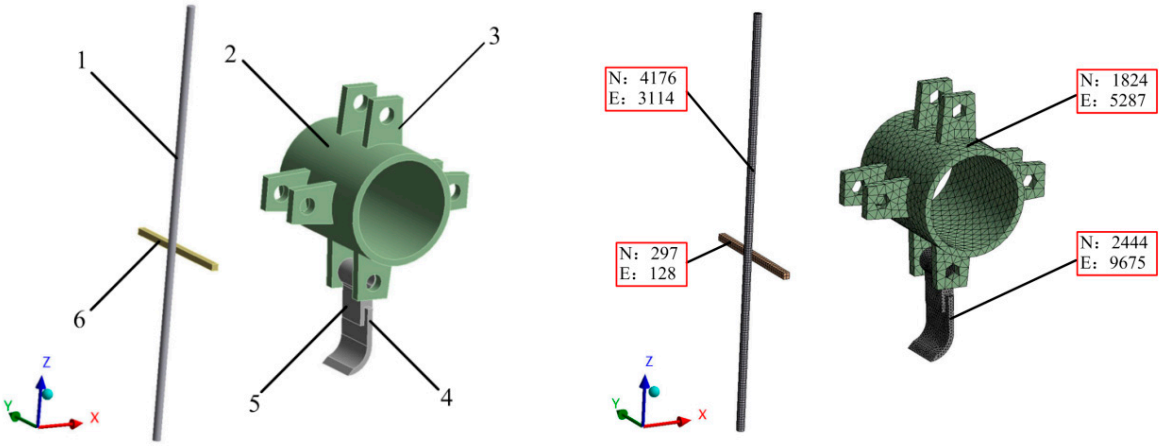

(**a**) Crushing model (**b**) Meshing grid

Figure 10. Cutting model and meshing grid: 1. Cotton stalk; 2. Cutter shaft; 3. Tool apron; 4. Cutter blade; 5. Connector; 6. Front baffle. N is the number of nodes, and E is the number of grid elements.

The overall meshing quality was good, the average element quality was 0.82, and the general requirement for the element quality was for it to be greater than 0.7. In addition, the average value of the aspect ratio was 1.93, and the aspect ratio was required to be between 1 and 5. The mean value of skewness was 0.26, and the meshing quality was better when the skewness was within the range of 0.25 to 0.5.

4.3. Crushing Model and Meshing Grid

A broken cotton stalk entered the crushing chamber with the rotation of the cutter blade, and it inevitably collided with and was torn by the cutter blades, fixed blades, front/back baffles, etc., resulting in the crushing of the cotton stalk. In order to reduce the amount of calculation required, only 12 cutter blades were used, and they were arranged on the cutter shaft (1000 mm in length) in a staggered way. Only the bent state of the cotton stalk was kept before cutting, as shown in Figure 11. The overall meshing quality was also good, the average element quality was 0.79, the average value of the aspect ratio was 1.93, and the mean value of the skewness was 0.26.

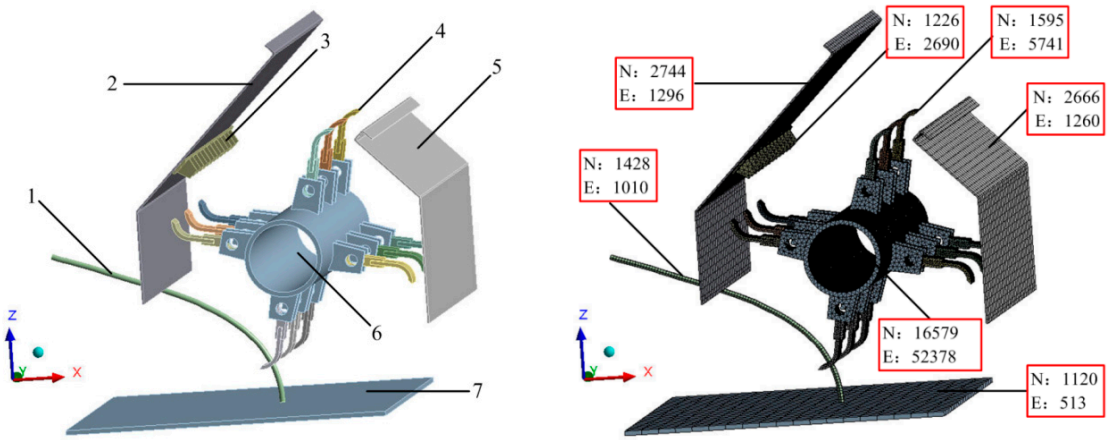

(**a**) Crushing model (**b**) Meshing grid

Figure 11. Crushing model and meshing grid; 1. Cotton stalk; 2. Front baffle; 3. Fixed blade; 4. cutter blade; 5. Back baffle; 6. Cutter shaft; 7. Ground. N is the number of nodes, and E is the number of grid elements.

4.4. Material Properties

According to the above analysis, a cotton stalk is a typical anisotropic material with a complex organizational structure [25]. It was only necessary to obtain the radial elastic modulus E_x (or E_y), axial elastic modulus E_z, axial shear modulus G_{xy}, radial shear modulus G_{xz} (or G_{yz}), Poisson's ratio u_{xy}, and Poisson's ratio u_{xz} (or u_{yz}). Then, the complete flexibility matrix could be determined, and the constitutive equation of a cotton stalk could be obtained. With reference to [26], nine independent elastic parameters of cotton stalk materials are shown in Table 1. In addition, the volume of a cotton stalk sample (ideal cylindrical shape) was measured with electronic vernier calipers, the mass was measured with an electronic balance, and the cotton stalk's density was calculated as 489.11 kg/m^3. Since cotton stalks have an elastic structure, the plastic-strain-failure mode was selected to simulate their failure. The evaluation index was expressed as the maximum equivalent plastic strain (EPS). Generally, the EPS of materials is no more than 20%.

Table 1. Elastic parameters of a cotton stalk.

E_x	E_y	E_z	G_{xy}	G_{xz}	G_{yz}	u_{xy}	u_{xz}	u_{yz}
MPa								
91.04	91.04	3181.79	28.45	180.88	180.88	0.6	0.025	0.025

E_x is the radial (x) elasticity modulus, E_y is the radial (y) elasticity modulus, E_z is the axial elasticity modulus, G_{xy} is the axial torsional shear modulus, G_{xz} is the radial (y) bending shear modulus, G_{yz} is the radial (y) bending shear modulus, μ_{xy} is Poisson's ratio (plane xy), μ_{xz} is Poisson's ratio (plane xz), and μ_{yz} is Poisson's ratio (plane yz).

All cutting and crushing components were rigid bodies (the cotton stalk was a flexible body) that would not be deformed in the process of movement. In order to reduce the amount of calculation that was required, structural steel was adopted for the cutting and crushing components, and the material properties of this structural steel were as follows: the modulus (density) was 7.85 $\times$ 10^3 kg/m^3, Young's modulus was 2 $\times$ 10^5 MPa, Poisson's ratio was 0.3, the bulk modulus was 1.67 $\times$ 10^5 MPa, and the shear modulus was 7.69 $\times$ 10^5 MPa.

4.5. Contact and Constraints

The contact between the cotton stalks and cutting blades was set as a body interaction, and the contact type was frictional. A self-made panel inclinometer with a universal angle ruler was used to measure the panel tilt angle. When the cotton stalk samples began to slide and roll, the tilt angles of the panels were 32.61° and 12.57°, respectively;

then, the kinetic and static friction coefficients were 0.22 and 0.64, respectively. After the experiment was completed, a drying treatment was carried out until the mass was no longer reduced, and the moisture content was calculated according to the mass before drying. The moisture content of the cotton stem samples was between 3.5% and 12.0%. The cotton stalks' contact properties were set to "eroding", and the contact equation was "ERODING_SINGLE_SURFACE". The cotton stalks' roots were fully restrained to simulate their growth. The connector and tool apron were connected in the "fixed-body-to-body" mode, and the pin shaft was omitted. Finally, the simulation results showed that the ratio of the hourglass energy to the total internal energy of the model was less than 5%, indicating that the parameters were reasonably set, the simulation model was effective, and it could reflect the cutting and crushing processes of cotton stalks to a certain extent.

5. Simulation Results and Analysis

5.1. Simulation Results for Cutting

Boundary conditions: The velocity of the front baffle and cutter shaft along the negative direction of the *x* axis was set to 1500 mm/s, and the cutter shaft's rotation speed was set to 1800 RPM. The cutting process was as follows: with the advance of the machine, cotton stalks first made contact with the front baffle; the stalks started in an upright state (a) and gradually underwent a bending deformation (b) until they made contact with the cutter blade, and the stalks were instantly cut off (c). Then, the cotton stalks' root ends (breakpoint #3699) entered the crushing chamber first (d) for the next stage of the crushing operation, as shown in Figure 12.

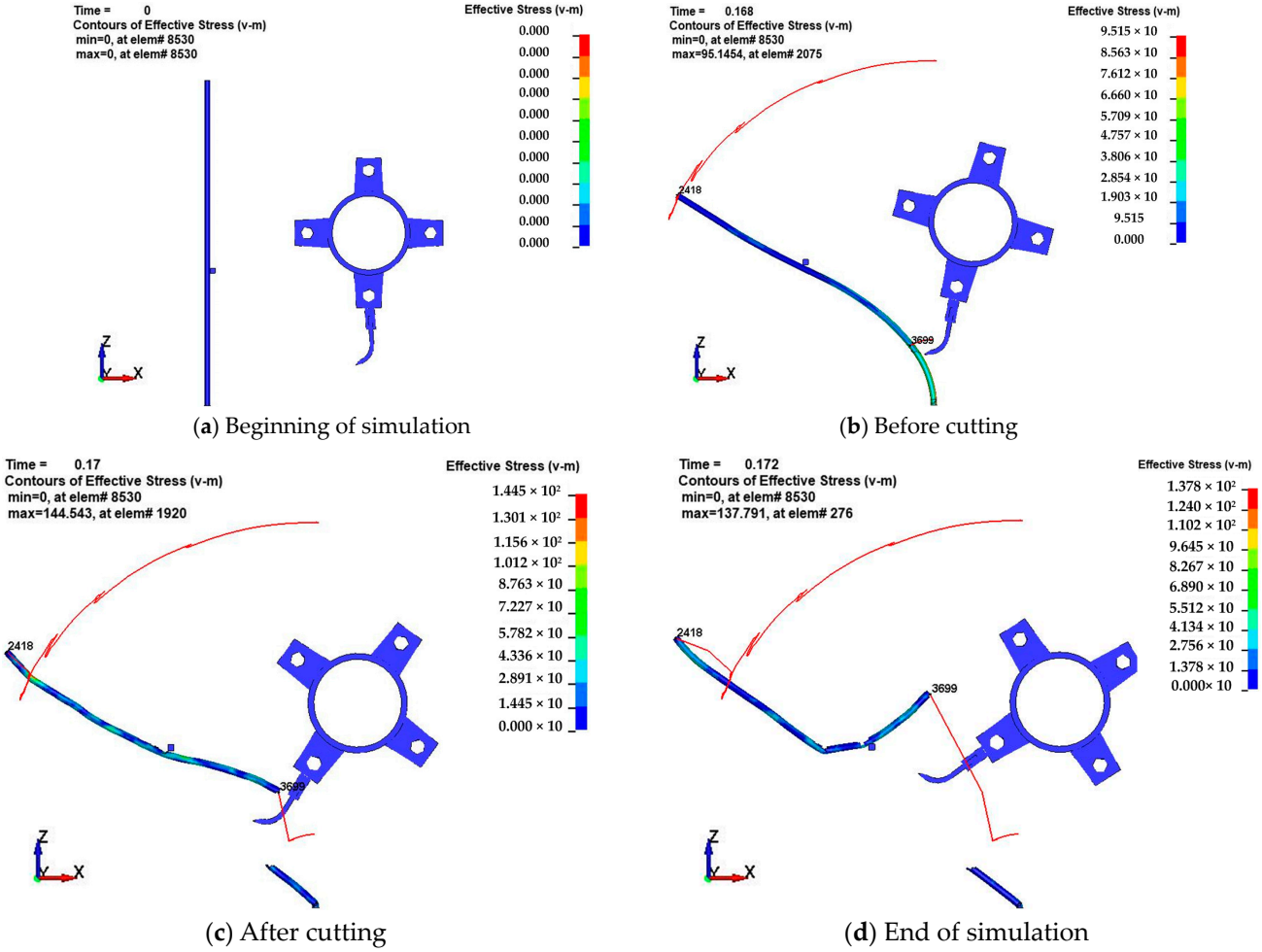

(**a**) Beginning of simulation (**b**) Before cutting

(**c**) After cutting (**d**) End of simulation

Figure 12. Cutting process for cotton stalks.

5.1.1. Equivalent Stress and Velocity Variations

Before the cotton stalks were cut, with the advance of the machine, they were gradually bent from their upright state. The tops of the cotton stalks were deformed the most. Changes in the cotton stalks' potential energy were ignored. The front baffle performed work on the cotton stalks, which was converted into the internal energy E_i and kinetic energy E_k of the cotton stalk. There were no significant changes in the stalks' kinetic energy until they made contact with the cutter blade.

With the advance of the machine, the stress on the cotton stalks' root ends gradually increased. Due to the extension of the outside (the side that made contact with the cutter blade) and the compression of the inside of the cotton stalks' root ends, the deformation of the tops of the cotton stalks was the greatest, and the internal energy gradually increased. At 0.17 s, the cutter blade collided with the cotton stalk at a high speed, and the average equivalent stress on the stalk reached a maximum value of 17.68 MPa; the stalk was instantly cut, and it was broken with a high initial velocity. The average velocity of the broken stalk reached a maximum value of 49.3 m/s, as shown in Figure 13.

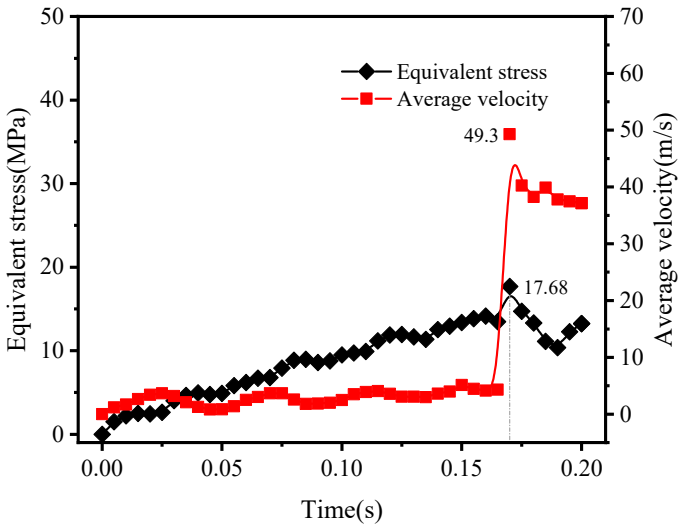

Figure 13. Equivalent stress and velocity variations of the cotton stalks.

5.1.2. Contact Force and Energy Variations

During the cutting process, the contact force in the x direction played a dominant role. At the moment of cutting, the maximum value of the contact force was 666.21 N. The kinetic energy and internal energy instantaneously increased, and the kinetic energy reached a maximum value of 46.935 J. Then, the impact force between the cutter blade and the stalks ended, the contact force instantly dropped to 0 N, and the speed and kinetic energy of the broken stalks were both decreased, as shown in Figure 14.

5.1.3. Effect of the Cutting Edge Angle (γ) on Stalk Cutting

When $\gamma \geq 55°$, the cotton stalks could not be effectively cut, which was not conducive to the subsequent straw-crushing operation. Therefore, 55°, 50°, 45°, and 40° were selected for a single-factor simulation test. As γ increased, the contact force gradually increased, as shown in Figure 15. However, γ could not be too small; otherwise, the thickness of the cutting edge was not sufficient, resulting in a low-strength and reduced service life. The broken stalks gained a high instantaneous velocity after being cut, and the kinetic energy increased. The greater the kinetic energy obtained, the more favorable it was for the broken stalks to enter the crushing chamber. The instantaneous kinetic energy obtained by the broken stalks decreased with the increase in γ. After comprehensive consideration, the angle was finally determined to be $\gamma = 45°$.

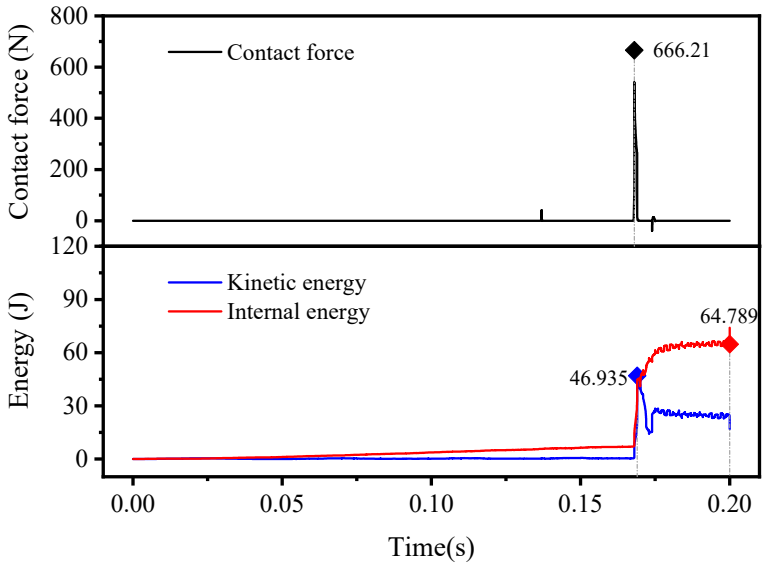

Figure 14. Contact force and energy variations of the cotton stalks.

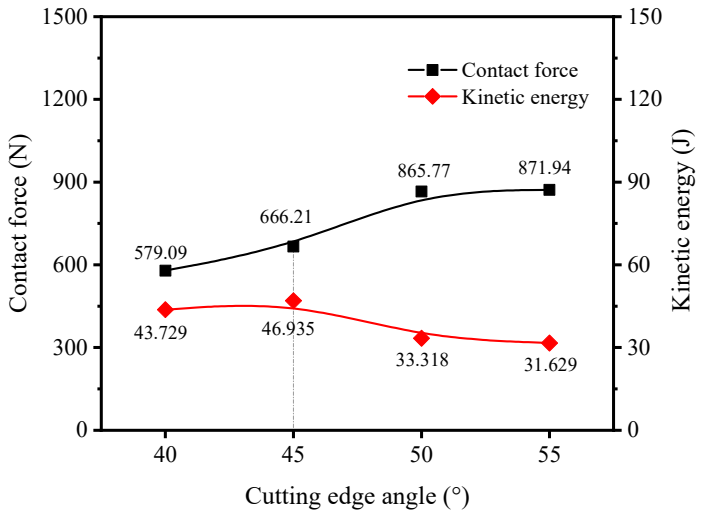

Figure 15. Effect on the cutting of cotton stalks due to the cutting edge angle.

5.1.4. Effect of the Front Baffle Height (h_1) on Stalk Cutting

In the simulation tests, if h_1 was greater than 280 mm, the cotton stalks could not be effectively cut, and the broken stalks flew forward, which was not conducive to the subsequent straw-crushing operation. In addition, h_1 should not be too small; otherwise, the high-speed air that would be generated might adsorb the residual film, thus aggravating the damage to the film's surface, which would not be conducive to the subsequent recovery of the residual film. In this section, h_1 = 280 mm, 265 mm, and 250 mm were selected for a single-factor simulation test. The height h_1 had little influence on the contact force, which first increased and then decreased, as shown in Figure 16.

With the increase in h_1, the instantaneous kinetic energy obtained by the cotton stalks first increased and then decreased. The maximum kinetic energy of the cotton stalks was obtained when h_1 = 265 mm, which was more conducive for the stalks to enter the crushing chamber, and the contact force was also at its maximum. After comprehensive consideration, the front baffle height was finally determined to be h_1 = 265 mm.

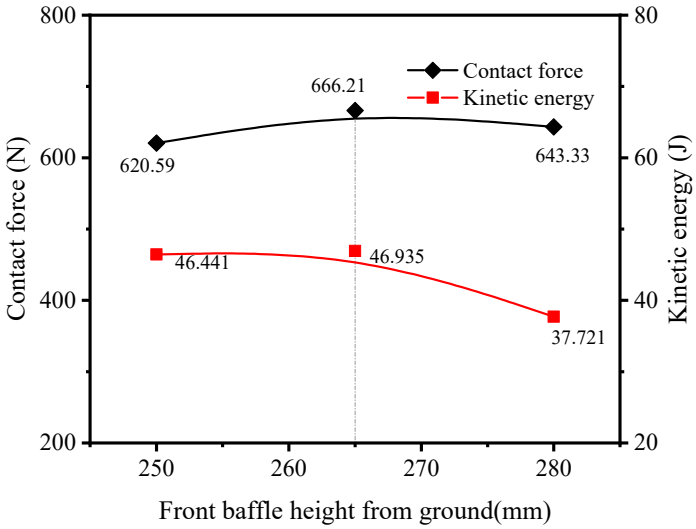

Figure 16. Effect on the cutting of cotton stalks due to the front baffle height.

5.1.5. Effect of the Cutter's Rotational Speed n on Stalk Cutting

With the other conditions (γ = 45°, h_1 = 265 mm, v_0 =1500 mm/s) remaining unchanged, only the cutter's rotational speed n was varied. When the rotational speed n was lower than 1600 RPM, the cotton stalks could not be effectively cut, which was not conducive to the subsequent crushing operation. Moreover, a rotational speed of n = 1800 RPM was chosen, and a simulation test was carried out under the conditions of n = 1600 RPM, 1800 RPM, and 2000 RPM. The effect of the cutter's rotational speed on stalk cutting was studied.

As shown in Figure 17, with the increase in the rotational speed n, the maximum contact force on the stalks gradually increased, and this was positively correlated with the rotational speed. The corresponding maximum contact forces under different rotational speeds were 442.65 N, 666.21 N, and 788.93 N, respectively. In other words, the greater the rotational speed n, the stronger the destructive power on the cotton stalks and the more favorable the cutting of the cotton stalks. Meanwhile, with the increase in the rotational speed n, the maximum kinetic energy of the stalks gradually increased, and the corresponding maximum kinetic energies at different rotational speeds were 26.919 J, 46.935 J, and 55.127 J, respectively. In other words, the higher the rotational speed n was, the more conducive it was for the cut stalks to enter the crushing chamber.

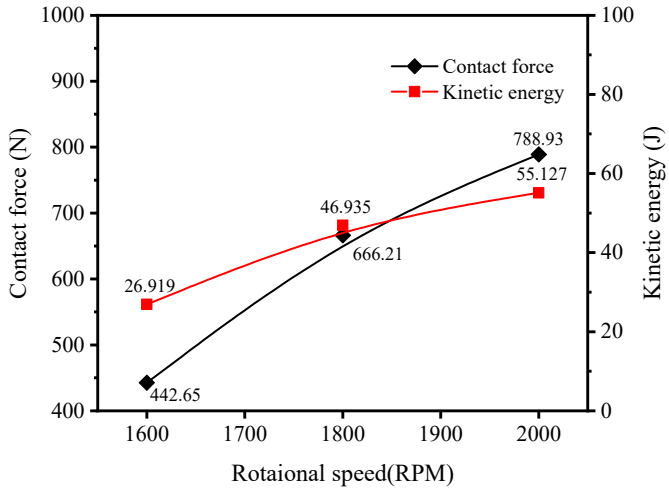

Figure 17. Effects on the cutting of cotton stalks due to the cutter's rotational speed.

5.1.6. Effects of the Machine's Forward Speed v_0 on Stalk Cutting

With the other conditions ($\gamma = 45^\circ$, $h_1 = 265$ mm, $n = 1800$ RPM) remaining unchanged, only the machine's forward speed v_0 was varied. Simulation tests were carried out under the conditions of $v_0 = 1000$ mm/s, 1500 mm/s, and 2000 mm/s to study the effects of the machine's forward speed on stalk cutting.

As shown in Figure 18, the forward speed had little effect on the maximum contact force at the moment of stalk cutting, and the corresponding maximum contact forces at different forward speeds were 659.05 N, 666.21 N, and 660.75 N, respectively. However, the maximum kinetic energy received at the moment of stalk cutting increased with the increase in the forward speed, and the increasing trend was obviously weaker than the influence of the rotational speed. The corresponding maximum kinetic energies at different forward speeds were 37.129 J, 46.935 J, and 51.915 J, respectively, indicating that the increase in forward speed was also conducive to the smooth entry of the cut stalks into the crushing chamber. Next, we proceed to the subsequent stage of the crushing operation.

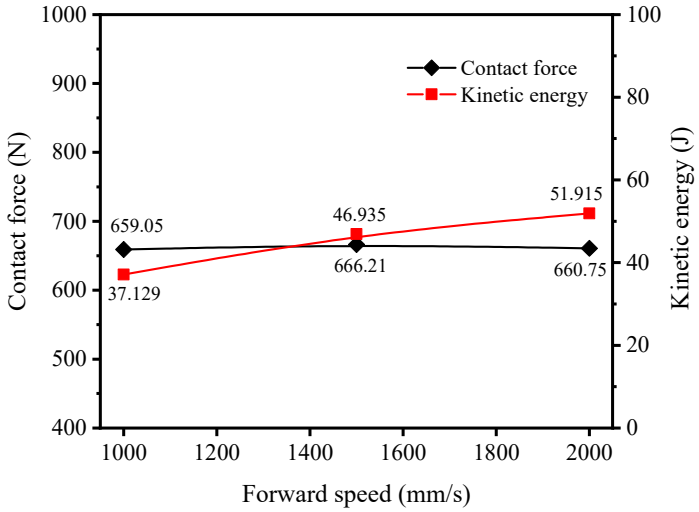

Figure 18. Effects on the cutting of cotton stalks due to the forward speed.

5.2. Simulation Results for Crushing

The starting point of the crushing process was the moment of contact between the cutter blade and the cotton stalks. Because the linear velocity of the cutter blade's edge (wR) was much larger than the forward speed (v_0), the forward speed of the machine was ignored, that is, the forward speed of the machine was $v_0 = 0$ m/s. The crushing process for cotton stalks was illustrated by taking the cutter shaft's rotation speed of $n = 2000$ RPM as an example, as shown in Figure 19.

At 0.0325 s, the rotating cutter blade collided with the cotton stalk at a high speed, and the initial cutting was completed at the bottom node #1339. The stubble height was about 93.2796 mm.

Subsequently, at 0.045 s, the whole broken stalk was rapidly deflected; node #1195 at the bottom of the broken stalk had a certain initial velocity, and it was the first to enter the crushing chamber with the cutter blade. The cutter blade collided with the cotton stalk at the bottom node #1145, thus completing the preliminary crushing. The length of the crushed straw was about 62.5878 mm.

At 0.0525 s, the crushed straw was thrown out of the crushing chamber at a certain speed, the broken stalk continued to move upward, and the topmost node #817 was deflected toward the lower part of the crushing chamber.

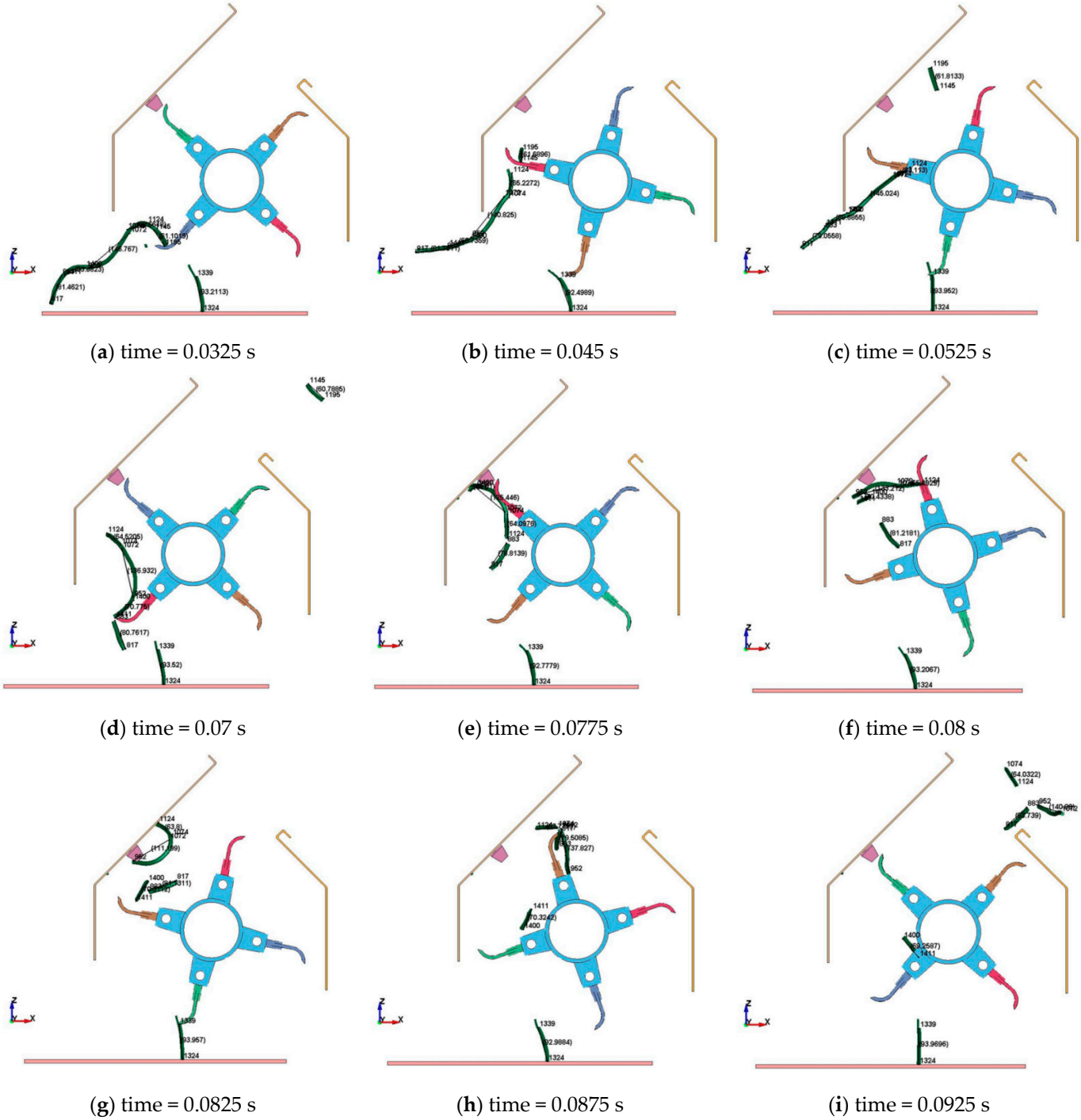

(**a**) time = 0.0325 s (**b**) time = 0.045 s (**c**) time = 0.0525 s

(**d**) time = 0.07 s (**e**) time = 0.0775 s (**f**) time = 0.08 s

(**g**) time = 0.0825 s (**h**) time = 0.0875 s (**i**) time = 0.0925 s

Figure 19. Crushing process for a cotton stalk.

At 0.07 s, collision and cutting occurred between the cutter blade and the cotton stalk at the topmost node #883, and further crushing was completed. The length of the crushed straw was about 81.1233 mm. The broken straw and the crushed straw continued to move upward into the crushing chamber.

At 0.0775 s, the broken straw moved to the fixed blade, which hindered the continued movement of the broken straw and played a supporting role.

At 0.08 s, the cutter blade collided with the cotton stalk at node #1400 to further complete the crushing. The length of the crushed straw was about 69.2696 mm. The broken and crushed straw continued to move upward.

At 0.0875 s, the cutter blade collided with the cotton stalk at node #1072, and the straw was further crushed into two parts; the lengths of the two parts of the crushed straw were 150.398 mm and 63.3354 mm, respectively.

At 0.0925 s, most of the crushed straw left the crushing chamber at a certain initial speed and was thrown out. Some straw (node #1400 and node #1411) was not sent out in time.

5.2.1. Equivalent Stress and Velocity Variations

The trends of the variations in the equivalent stress and average velocity of the cotton stalk during the process of crushing were basically consistent. The greater the equivalent stress that occurred at the moment of contact with the cutter blade, the greater the velocity obtained at the moment after the collision. The higher the equivalent stress was, the more favorable the stalk crushing would be, and the higher the average velocity was, the more favorable it would be for the stalk to be thrown out. At 0.0925 s, the maximum equivalent stress on the stalk was 7.758 MPa. At 0.1 s, the maximum average velocity of the stalks was 53.429 m/s, as shown in Figure 20.

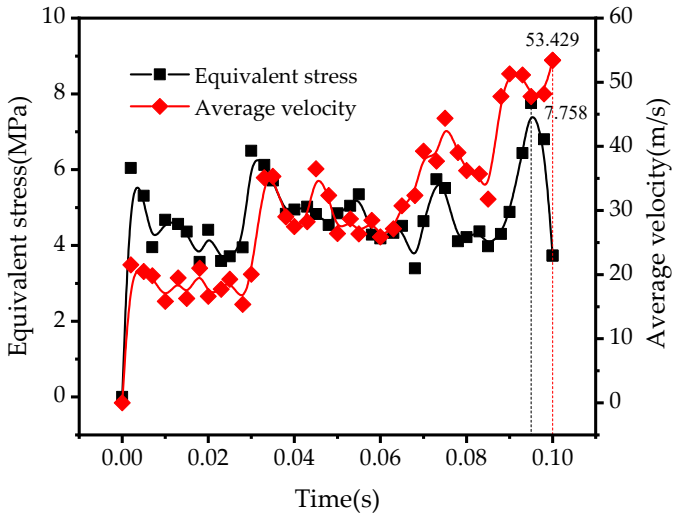

Figure 20. Equivalent stress and velocity variations of the cotton stalk.

5.2.2. Contact Force and Energy Variations

Figure 21 shows the contact force, kinetic energy, and internal energy obtained during the crushing process for the cotton stalk. During the crushing process, the internal energy of the stalk gradually increased and reached a maximum of 113.51 J. The variations in kinetic energy were closely related to the impact of the cutter blade on the stalk. The kinetic energy immediately increased at the moment of stalk cutting and reached a maximum of 31.73 J. The greater the kinetic energy was, the better the stalk would be crushed and thrown out. It was found that, due to the complex posture of the stalk in the crushing chamber, the angle between the stalk and the x-axis was larger than that between the stalk and the z-axis, and the contact force in the x-direction was dominant. Conversely, the contact force in the z-direction was dominant. The maximum contact forces were 739.01 N, 678.68 N, 1292 N, and 1098.5 N before the stalk was cut.

Therefore, within 0.1 s, the cotton stalk was cut, entered the crushing chamber, and thrown out. According to the requirements for working quality from NYT 500-2015: "Operating quality for straw-smashing machines", the qualified length of a crushed cotton stalk should not exceed 200 mm. The simulation results showed that the lengths of the crushed cotton stalks were 62.5878 mm, 81.1233 mm, 69.2696 mm, 150.398 mm, and 63.3354 mm. The maximum length of a cotton straw was 150.398 mm (the distance between node #1072 and node #1124), which was not more than 200 mm, that is, the qualified crushing rate

was 100%. According to the simulation results, the straw did not fall on the ground after crushing, and the straw removal effect reached 100%.

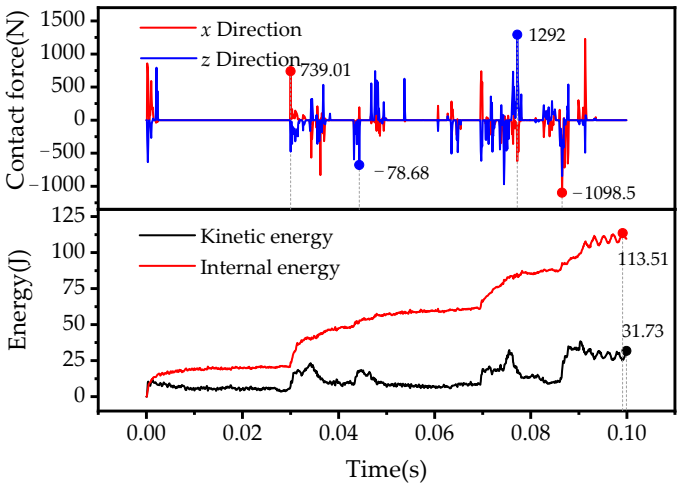

Figure 21. Contact force and energy variations of the cotton stalk.

5.2.3. Effect of the Cutter's Rotational Speed on Straw Smashing

When the cotton stalk was cut and entered the crushing chamber, the stalk and the machine were relatively stationary in the direction of advance, so the rotation speed of the cutter was the key working parameter affecting the smashing and throwing of the straw. The designed rotation speed of the machine was 1800 RPM, and single-factor simulation tests were carried out. Five tests were conducted with the three rotational speeds (n = 1600 RPM, 1800 RPM, and 2000 RPM) to study the influences of different rotational speeds on the rate of qualified cotton stalk crushing and the effects on straw removal. The qualified crushing rate η_0 and the removal rate ε_0 were calculated with the following formula:

$$\begin{cases} \eta_0 = \frac{650-L_C-L_U}{650-L_C} \times 100\% \\ \varepsilon_0 = \frac{650-L_C-L_R}{650-L_C} \times 100\% \end{cases} \quad (6)$$

where L_C is the stubble height (mm), L_U is the unqualified length of crushed stalks (mm), L_R is the length of stalks that fall on the ground (mm), and 650 is the length of the cotton stalk model (mm).

At the end of the 15 simulation tests, the number of stalks produced and the lengths of the crushed stalks were different at different cutter-shaft rotation speeds. At low rotational speeds, the number of crushed stalks (21) was significantly lower than that at high rotational speeds (27), as shown in Figure 22. Moreover, the number of stalks with lengths greater than 200 mm was significantly increased at low rotational speeds, which directly resulted in a decrease in the rate of qualified stalk crushing. The main reason was that with the increase in the cutter shaft's rotational speed, the probability of collision between the cutter blade and cotton stalks increased, and the number of stalks produced via crushing increased. With the increase in the rotational speed of the cutter shaft, the average speed of the straw obtained after crushing increased. The average straw speeds obtained at 1600 RPM, 1800 RPM, and 2000 RPM were 30.82 m/s, 35.47 m/s, and 37.27 m/s, respectively. Therefore, the kinetic energy of the stalk increased accordingly, and this was more conducive to the throwing of the stalk after crushing to achieve the purpose of stalk removal. According to the data in Figure 22 and Formula (6), the rate of qualified crushing and the removal rate under different rotational speeds were calculated. With the increase in the cutter shaft's speed, the rate of qualified crushing and the removal rate were both increased. The effect of the cutter shaft's speed on the rate of qualified cotton stalk crushing was significant.

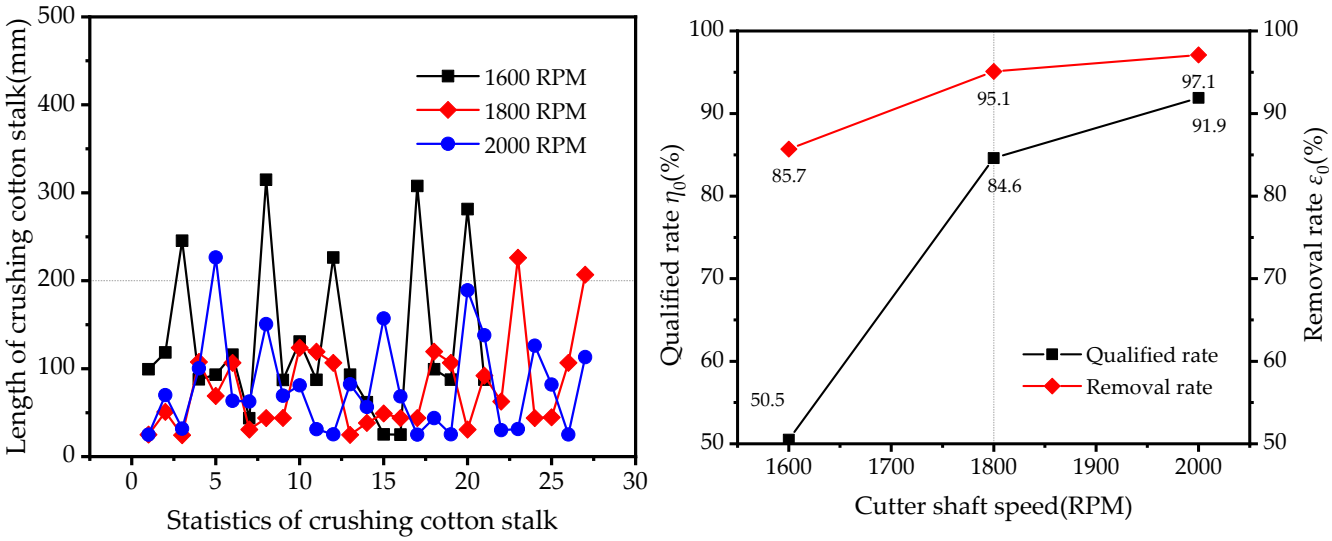

Figure 22. Effects of the cutter shaft's speed on cotton stalk crushing.

6. Field Experiment

6.1. Test Conditions

Hansen Machinery Co., Ltd., Changzhou city, Jiangsu province, China. That completed the manufacturing and installation of the device according to the design scheme, as shown in Figure 23. The prototype was safe in its operation, the design of the mechanical structure was reasonable, the components did not interfere with each other, and there was no obvious vibration or noise.

Figure 23. Trial production of the prototype.

In order to test the field performance of the device and the reliability of its working process, a field experiment was carried out in the 10th Regiment of the First Division of the Xinjiang Corps. The test field was an area for demonstrating the application of plastic-film-recovery technology and equipment. After cotton was harvested, the irrigation belts were manually removed, and the test field's area was about 20 ha. The cotton variety was "Zhongmian 70", and the soil type was sandy. The thickness of the plastic film used was 0.01 mm, and its width was 2050 mm. The supporting power was a Revo M 904-D tractor with a power of 66.2 kW.

6.2. Test Indexes and Method

According to the agronomic design requirements for the test methods and performance indexes for crushing and returning cotton straw to a field in NY/T 500-2015: "Operation quality for straw-smashing machines", the stubble height should not be higher than 80 mm, and the rate of qualified cotton straw crushing should not be less than 85% (the qualified length of cotton straw should not exceed 200 mm). In addition, the effect of the removal of

impurities from the film surface was the focus of this study; these impurities were mainly composed of light impurities and cotton straw, and the film's content of thrown straw needed to be considered at the same time. Therefore, the stubble height, rate of qualified straw crushing, film-surface-impurity clearance rate, and film content were selected as experimental indexes for this field experiment.

6.2.1. Stubble Height Y_1

Under the test conditions, after the straw-crushing operation, five points were measured in the direction of the length of the test area (greater than 100 m), and the stubble heights of three stalks were measured within the range of 1 m × 1 m at each point by using steel measuring tape with an accuracy of 1 mm, the average of which was the stubble height at the test point. The average stubble height of the five measuring points was taken as the stubble height under these test conditions. So, the stubble height could be expressed as

$$Y_1 = \frac{1}{3 \times 5} \sum y_{ij} \tag{7}$$

In the formula, Y_1 is the stubble height (mm); y_{ij} is the stubble height of each straw measured at each measuring point (i = 1,2 . . . , 5; j = 1,2,3). The collection of the stubble height data is shown in Figure 24a.

(**a**) Stubble height measurement

(**b**) Collecting straw

(**c**) Collecting the impurities

(**d**) Collecting the residual film

Figure 24. Acquisition of test data.

6.2.2. Rate of Qualified Straw Crushing Y_2

Under the test conditions, after the straw-crushing operation, five points were measured in the direction of the length of the test area (greater than 100 m), and the mass of all of the straw in the 1 m × 1 m range at each point was measured. The straw with an unqualified length was picked out and weighed by using an electronic scale with an accuracy of 1 g. The straw data collected from the measuring points are shown in Figure 24b. Under each working condition, the rate of qualified straw crushing Y_2 could be expressed as (i = 1,2 . . . , 5)

$$Y_2 = \frac{1}{5} \sum \frac{m_{zi} - m_{\mathrm{bi}}}{m_{zi}} \times 100\% \tag{8}$$

where Y_2 is the rate of qualified straw crushing (%); m_{zi} is the mass of all straw in the range of 1 m × 1 m (g); and m_{bi} is the mass of the straw with an unqualified length in the range of 1 m × 1 m (g).

6.2.3. Film-Surface-Impurity Clearance Rate Y_3

Through many field experiments, it was found that most of the impurities were thrown out by the crushing chamber, some of the impurities were with the recovered residual film,

and some of the impurities fell off in the field during the process of picking up the residual film. Then, the film-surface-impurity clearance rate of the device could be expressed as

$$Y_3 = \frac{M_p}{M_z} \times 100\% = \frac{M_p}{L \times \rho_Z} \times 100\% \quad (9)$$

where M_p is the mass of impurities that were thrown out (kg); M_z is the total impurity mass on the film's surface (kg); and ρ_Z is the film-surface-impurity quality per unit length (kg/m). Here, the value of ρ_Z = 2.532 kg/m was measured during the test. Due to the need to collect and measure the quality of the impurities that were thrown out, the length L of the test area should not have been too large every time. In this study, L = 30 m. The data collected on the impurities are shown in Figure 24c.

6.2.4. Film Content Y_4

Under the test conditions, after the straw-crushing operation, five points were measured in the direction of the length of the test area (greater than 100 m). The length of each measuring point was 5 m, and the width was one working width. Then, under each working condition, the film content Y_4 could be expressed as (i = 1,2 . . . , 5)

$$Y_4 = \frac{1}{5}\sum \frac{m_{pi}}{m_c} \times 100\% \quad (10)$$

where m_{pi} is the mass of the residual film thrown out at each measuring point (g); m_c is the residual film mass within the measuring-point length of 5 m (g). According to previous measurements, the residual-film mass per unit length of the film was about 64 g, so m_c = 5 × 64 = 320 g. The smaller Y_4 was, the better, as this indicated a greater residual-film recovery. Otherwise, it indicated that in the process of crushing and returning straw to the field, the film surface was sucked into the crushing chamber and thrown out. The residual film was collected and weighed, as shown in Figure 24d.

7. Results and Discussion

7.1. Experimental Results

The field experiments showed that the cutting of some cotton stalks was not good when the forward speed v_0 was too high. When the speed v_0 exceeded 7 km/h, the stubble height was too great. However, the speed v_0 could not be slower than 4.5 km/h, as this would seriously affect the working efficiency and would not allow the agronomic requirements to be met. When the cutter's rotational speed n exceeded 2000 RPM, too much broken film was thrown out, which indirectly resulted in a low rate of residual-film recovery. However, the rotational speed n should not be too low. When the rotational speed n was lower than 1600 RPM, the effect of the removal of impurities on the film's surface was not good, resulting in more impurities in the recovered residual film.

Considering the feasibility of the test operation, the forward speed of the machine was controlled at 5.5–6 km/h, and the rotational speed of the cutter shaft was controlled at 1850–1900 RPM during the test. Three repeated tests were carried out, and the average values were taken as the test values. The test results were as follows: the stubble height was 8.0 cm, the rate of qualified straw crushing was 91.8%, the clearance rate of film-surface impurities was 92.3%, and the film content was 3.6%, which met the working quality requirements (the stubble height should not be higher than 80 mm, and the rate of qualified cotton straw crushing should not be less than 85%) of NYT 500-2015: "Operating quality for straw-smashing machines". To some extent, the device met the requirements of agronomic design.

7.2. Discussion

It was not difficult to find that the results for the rate of qualified straw crushing and the film-surface-impurity clearance rate were in agreement with the results of the

simulations. The larger the rotational speed of the cutter shaft, the better the effects of straw crushing and impurity removal. This is because the higher rotational speed increased the probability of contact between the straw and the cutter blades (or fixed blades). Meanwhile, a higher rotational speed increased the linear velocity of the cutter blade's edge, and its cutting capacity and throwing capacity became stronger, making it more conducive to straw crushing and removal. This is why the results of straw crushing and removal in the above field tests were all satisfactory, and light impurities, such as cotton and cotton leaves, could not be seen in the recovered residual film.

In addition, it was found in the tests that there were few other impurities outside the crushed straw in the recovered residual film. Because the rotational speed was higher, the airflow velocity below the crushing chamber on the film's surface was greater, the ability to absorb impurities was stronger, and the effect on the removal of other impurities was better. Meanwhile, the residual film could easily be sucked up too. Once the residual film collided with the cutter blades, it was torn, broken, and thrown out with the impurities, which indirectly led to a lower rate of film recovery.

The height h_0 (of the cutter blade's edge from the ground) had an important influence on the velocity and pressure distribution in the crushing chamber, which affected the effect of the removal of impurities on the film's surface. The lower the height h_0, the greater the flow rate of the wind field on the film's surface, which could promote the removal of impurities on the film's surface but aggravated the risk of damaging it, resulting in a substantial increase in the film content. The greater the height h_0, the greater the stubble height if the height h_0 was more than 70 mm. However, the stubble height was greater than 80 mm. To reduce the film content and stubble height as much as possible, the height h_0 was adjusted to 7.0 cm.

8. Conclusions

The working principle and structure of a front-mounted cotton-straw-crushing device are described in detail in this study. The structural parameters of the key components, such as the cutter blade, fixed blade, and crushing chamber used to cut and crush cotton stalks, were designed.

The height h and dip angle α of the fixed blade were determined to be 30 mm and 75° through a finite element analysis. The maximum stress was 137.23 MPa, and the maximum deformation was 0.008 mm. Considering the tensile strength of the selected material and the minimum tensile strength of the weld metal, the design of the fixed blade was feasible. A cotton stalk is a typical anisotropic material with a complex organizational structure. A geometric model of a cotton stalk was established. On the basis of the device design, explicit dynamic models of the cutting and crushing of a single cotton stalk were established based on ANSYS/LS-DYNA. The results of the dynamic analysis revealed the cutting mechanism of the cotton stalk: the cutter blade collided with the cotton stalk at a high speed, the stalk was instantly cut, and the cotton stalk's root ends entered the crushing chamber first. The influence of the cutting edge angle γ and the front baffle height h_1 on cotton stalk cutting was studied with single-factor simulation tests. An edge angle of γ = 45° and a height of h_1 = 265 mm were determined, and the influences of the cutter's rotational speed and forward speed on cutting were also studied. Meanwhile, the mechanism of cotton straw crushing was revealed, and the motion states of the straw were studied at different times. By studying the influence of the cutter shaft's rotation speed on the rate of qualified straw crushing η_0 and removal rate ε_0, it was concluded that with an increase in the cutter shaft's speed, the rate of qualified crushing and the removal rate were both increased. At the design speed of n = 1800 RPM, the rate of qualified crushing was η_0 = 84.6%, and the removal rate was ε_0 = 95.1%.

Finally, under working conditions, the forward speed of the machine was controlled at 5.5–6 km/h, and the rotational speed of the cutter shaft was controlled at 1850–1900 RPM during the test. The test results were as follows: the stubble height was 8.0 cm, the rate of

qualified straw crushing was 91.8%, the clearance rate of film-surface impurities was 92.3%, and the film content was 3.6%.

Author Contributions: Conceptualization, methodology, data curation, formal analysis, writing original draft, writing review and editing, P.W. and X.C.; investigation, X.C.; data curation, H.W.; funding acquisition, X.C. and H.W.; validation, X.C.; supervision, H.W. All authors have read and agreed to the published version of the manuscript.

Funding: This research was funded by the Special Scientific Research Project for Public Welfare Industry of Ministry of Agriculture (201503105).

Institutional Review Board Statement: Not applicable.

Informed Consent Statement: Not applicable.

Data Availability Statement: All data are presented in this article in the form of figures and tables.

Conflicts of Interest: The authors declare no conflict of interest.

References

1. Gao, H.; Yan, C.; Liu, Q.; Ding, W.; Chen, B.; Li, Z. Effects of plastic mulching and plastic residue on agricultural production: A meta-analysis. *Sci. Total Environ.* **2019**, *651*, 484–492. [CrossRef] [PubMed]
2. Chen, B.; Cui, J.; Dong, W.; Yan, C. Effects of Biodegradable Plastic Film on Carbon Footprint of Crop Production. *Agriculture* **2023**, *13*, 816. [CrossRef]
3. Wang, P.; Chen, X.; Wen, H. Research and Experiment on the Removal Mechanism of Light Impurities of the Residual Mulch Film Recovery Machine. *Agriculture* **2022**, *12*, 775. [CrossRef]
4. Xie, C.; Kang, J.; Peng, Q.; Wang, X.; Chen, Y.; Zhang, C.; Zhang, N. Optimization of Screen-Hole-Clearing Devices for Mechanized Residual Film–Impurity Separation. *Appl. Sci.* **2022**, *12*, 11658. [CrossRef]
5. Peng, Q.; Li, K.; Wang, X.; Zhang, G.; Kang, J. Design and Test of Stripping and Impurity Removal Device for Spring-Tooth Residual Plastic Film Collector. *Agriculture* **2023**, *13*, 42. [CrossRef]
6. Cao, S.; Xie, J.; Wang, H.; Yang, Y.; Zhang, Y.; Zhou, J.; Wu, S. Design and Operating Parameters Optimization of the Hook-and-Tooth Chain Rail Type Residual Film Picking Device. *Agriculture* **2022**, *12*, 1717. [CrossRef]
7. Shi, X.; Niu, C.; Wang, X.; Zhang, H.; Yang, H. Design of roller sieve waste plastic film and trash winnowing machine. *Trans. Chin. Soc. Agric. Eng.* **2017**, *33*, 19–26.
8. Li, J. Study on the Water-Separating Device of Residual Film Mixture Collected by Machine. Master's Thesis, Shihezi University, Shihezi, China, 2018.
9. Tang, J.; Li, X.; Zhang, G.; Lu, W.; Ni, S.; Sun, Z.; Li, H.; Zhao, C.; Zhang, H.; Zhang, Q.; et al. An ANSYS/LS-DYNA Simulation and Experimental Study of Sectional Hob Type Laver Harvesting Device. *Agriculture* **2023**, *13*, 361. [CrossRef]
10. Duan, Y.; Yuan, D.; Wu, J.; Deng, X.; Wu, B.; Sun, Z. Effect of the Geometric Configuration of the Disc Cutter on the Cutting Behaviour in Tunneling. *Appl. Sci.* **2023**, *13*, 72. [CrossRef]
11. Cao, W.; Sun, W.; Niu, C.; Jiao, J.; Chen, B. Combed Safflower Picking Device Based on ANSYS/LS-DYNA. *Trans. Chin. Soc. Agric. Mach.* **2018**, *49*, 123–131.
12. Sun, J.; Xing, K.; Yang, Z.; Duan, J. Simulation and experimental research on fruit branch pruning process based on ANSYS/LS-DYNA. *J. South China Agric. Univ.* **2022**, *43*, 113–124.
13. Dun, G.Q.; Yang, Y.Z.; Li, H.S. Working parameters optimization of soybean serration rotarycutter by ANSYS/LS-DYNA. *J. Henan Agric. Univ.* **2019**, *53*, 739–744.
14. Shi, J.; Chen, F.; Guo, J.; Wang, X. Design and experimental research of the field straw chopper with throwing cotton-stalk. *Trans. Chin. Soc. Agric. Eng.* **2006**, *22*, 68–72.
15. Zhang, Z.; He, J.; Li, H.; Wang, Q.; Ju, J.; Yan, X. Design and Experiment on Straw Chopper Cum Spreader with Adjustable Spreading Device. *Trans. Chin. Soc. Agric. Mach.* **2017**, *48*, 76–87.
16. Qin, K.; Cao, C.; Liao, Y.; Wang, C.Q.; Fang, L.F.; Ge, J. Design and optimization of crushing and throwing device for straw returning to field and fertilizing hill-seeding machine. *Trans. Chin. Soc. Agric. Eng.* **2020**, *36*, 1–10.
17. Zhang, X.; Wang, Z.; Li, Y.; Liang, D. Design and experiment of sliding-cutting and anti-twining returning device for banana straw. *Trans. Chin. Soc. Agric. Eng.* **2018**, *34*, 26–34.
18. Chinese Academy of Agricultural Mechanization Science. *Agricultural Machinery Design Manual*; Agricultural Science and Technology Press: Beijing, China, 2007; Volume 1.
19. Yu, Y.; Chen, X.; Wen, H. Development and experiment of straw chopping and plastic film strip-collection combined machine. *Trans. Chin. Soc. Agric. Eng.* **2016**, *32*, 1–8.
20. Ding, L. Design and Experimental Study on Saw Type Cotton Stalk Cutting Test Bench. Master's Thesis, Shihezi University, Shihezi, China, 2015.

21. Zheng, Z.; He, J.; Li, H.; Diao, P.; Wang, Q.; Zhang, C. Design and Experiment of Straw-chopping Device with Chopping and Fixed Knife Supported Slide Cutting. *Trans. Chin. Soc. Agric. Mach.* **2016**, *47*, 108–116.
22. Pu, L.; Ji, M. *Mechanical Design*, 8th ed.; Higher Education Press: Beijing, China, 2006; pp. 120–126.
23. Jiménez-Armendáriz, J.; Jimenez-Martinez, M.; Varela-Soriano, J.; Santana-Diaz, A.; Perez-Santiago, R. Energy Dissipation Enhancement of Thin-Walled 6063 T5 Aluminium Tubes by Combining a Triggering Mechanism and Heat Treatment. *Metals* **2023**, *13*, 922. [CrossRef]
24. Tian, X.; Zhao, Y.; Chen, X.; Yan, L.; Wen, H.; Gou, H.; Ji, C. Development of 4JSM-2000A type combined operation machine for cotton stalk chopping and residual plastic film collecting. *Trans. Chin. Soc. Agric. Eng.* **2018**, *34*, 25–35.
25. Shi, N. Peeling Method of Cotton Stalk and Development of Rubbing Peeling Machine. Doctor's Thesis, Northwest A & F University, Yangling, China, 2014.
26. Zhao, W.; Xie, J.; Wang, Z.; Gao, Q.; Chen, M. Investigation of mechanical properties of cotton stalk based on multi-component analyses. *Int. Agrophys.* **2022**, *36*, 257–267. [CrossRef]